

The Effects of Zirconia Morphology on Methanol Synthesis from CO and H<sub>2</sub>  
over Cu/ZrO<sub>2</sub> Catalysts: Part II – Transient-Response Infrared Studies

Michael J. Rhodes, Konstantin Pokrovski, and Alexis T. Bell\*

Chemical Sciences Division  
Lawrence Berkeley National Laboratory  
and  
Department of Chemical Engineering  
University of California  
Berkeley, CA 94720-1462

Submitted to  
Journal of Catalysis

March 21, 2005

Author to whom correspondence should be addressed: [bell@cchem.berkeley.edu](mailto:bell@cchem.berkeley.edu)

## Abstract

The interactions of CO, CO/H<sub>2</sub>, H<sub>2</sub>, D<sub>2</sub>, and CH<sub>3</sub>OH with t-ZrO<sub>2</sub>, m-ZrO<sub>2</sub>, Cu/t-ZrO<sub>2</sub>, and Cu/m-ZrO<sub>2</sub> have been investigated by *in-situ* infrared spectroscopy with the aim of understanding the nature of species involved in methanol synthesis and the dynamics of the formation and consumption of these species. With both phases of ZrO<sub>2</sub>, the primary surface species observed during CO hydrogenation were bidentate formate groups, b-HCOO-Zr, and methoxide groups, CH<sub>3</sub>O-Zr. Transient-response experiments indicated that the rate-limiting step for each catalyst is the reductive elimination of methoxide species. Relative to 1.2 wt% Cu/t-ZrO<sub>2</sub>, though, spillover of H atoms and the formation and reduction of formate and methoxide species proceeded more rapidly on the more active 1.2 wt% Cu/m-ZrO<sub>2</sub>. Steady-state intensities of surface species were also larger on 1.2 wt% Cu/m-ZrO<sub>2</sub>. These differences are attributed to the higher reactivity of the hydroxyl groups on the surface of m-ZrO<sub>2</sub>. Increasing the Cu surface area on m-ZrO<sub>2</sub> increases the rate of reductive elimination of methoxide species up to a maximum value, determined by the eventual saturation of the ZrO<sub>2</sub> surface with H atoms via spillover from Cu. The product of the apparent rate coefficient for reductive elimination of methoxide species and the surface concentration of these species increases linearly with increasing Cu surface area consistent with the proportionality seen in the rate of methanol synthesis at steady state.

## Introduction

Cu supported on  $\text{ZrO}_2$  with Cu is a very active catalyst for the synthesis of methanol from CO and  $\text{H}_2$  [1-11]. Previous studies have shown that both catalyst components play a role in the hydrogenation of CO to methanol –  $\text{ZrO}_2$  adsorbs CO and all carbon-containing intermediates leading to methanol, whereas supported Cu particles adsorb  $\text{H}_2$  and then spillover H atoms onto the surface of  $\text{ZrO}_2$  where they participate in the hydrogenation of CO. In Part I of the present study we demonstrated that the phase of  $\text{ZrO}_2$  has a strong influence on catalyst activity and selectivity [12]. Catalysts prepared using monoclinic  $\text{ZrO}_2$  (m- $\text{ZrO}_2$ ) are nearly an order of magnitude more active for methanol synthesis activities and exhibit higher methanol selectivities than catalysts with the same Cu surface density deposited on tetragonal  $\text{ZrO}_2$  (t- $\text{ZrO}_2$ ) having the same surface area as m- $\text{ZrO}_2$ . These differences are attributed to the higher concentration of anionic defects on m- $\text{ZrO}_2$  than t- $\text{ZrO}_2$ . Such defects when present adjacent to surface hydroxyl groups readily adsorb CO to form bidentate formate groups. It was also shown that the methanol synthesis activity of Cu/ $\text{ZrO}_2$  is proportional to the surface area of the deposited Cu. Increasing the overall Cu surface area increases the rate of H atom spillover and, hence, the rate of hydrogenation of adsorbed CO to methanol.

In Part II of this study, *in-situ* FTIR spectroscopy was utilized to investigate the dynamics of CO adsorption and CO hydrogenation on Cu/m- $\text{ZrO}_2$  and Cu/t- $\text{ZrO}_2$  at reaction temperature. This work was undertaken to determine the nature of the adsorbed species formed and their relationship to the mechanism of methanol synthesis. These transient-response studies also provided insights into relative rates at which elementary

processes occur on Cu/m-ZrO<sub>2</sub> and Cu/t-ZrO<sub>2</sub>. The effects of the concentration of exposed Cu atoms on the dynamics of CO hydrogenation were also investigated.

## Experimental

The preparation and characterization of the Cu/ZrO<sub>2</sub> catalysts used in this study have been described previously [12]. Both t-ZrO<sub>2</sub> and m-ZrO<sub>2</sub> have a surface area of ~ 145 m<sup>2</sup>/g. Cu was deposited on each support by deposition-precipitation, which was found to a higher dispersion of Cu compared to incipient-wetness impregnation [13]. The surface areas of the dispersed Cu was determined by H<sub>2</sub>-TPR following N<sub>2</sub>O titration [13], the results are presented in Table 1.

The steady-state methanol synthesis activity of each sample was measured using a glass-lined microreactor. A 3/1 mixture of H<sub>2</sub> and CO was supplied to the reactor from a gas manifold and the reaction products were analyzed by gas chromatography. A more detailed description of the reactor apparatus is given in ref. [12]. Steady-state rate data were collected at 523 K, a total pressure of 3.0 MPa, and a feed flow rate of 60 cm<sup>3</sup>/min.

*In-situ* transmission infrared spectroscopy experiments were conducted using a low-dead-volume infrared cell equipped with CaF<sub>2</sub> windows [14]. Samples were pressed into pellets with a density of approximately 0.015 g/cm<sup>3</sup>. Infrared spectra were collected using a Nicolet Magna 750 series II FTIR spectrometer equipped with a narrow-band MCT detector. *In-situ* absorbance spectra were obtained by collecting either 32 or 128 scans at 2 cm<sup>-1</sup> resolution, which were then referenced to a spectrum of the catalyst taken after pretreatment in flowing He at the same temperature as that used for reaction. The cell was heated by electrical resistance heaters, controlled by a programmable

temperature controller (Omega), and the sample temperature was monitored by a thermocouple located just above the catalyst pellet inside the cell.

The reactants used for the infrared experiments were purified prior to delivery to the sample cell. H<sub>2</sub> (99.999%) [Airgas] was purified using Oxi-Clear (Alltech) traps to remove O<sub>2</sub> and H<sub>2</sub>O. He (99.999%) was passed through a synthetic zeolite adsorbent (Alltech) to remove CO, CO<sub>2</sub>, O<sub>2</sub>, and H<sub>2</sub>O impurities. Another molecular sieve trap (Alltech) was used to remove CO<sub>2</sub> and H<sub>2</sub>O from 15% CO/He (99.99%) [Airgas]. The purified gases were delivered to the infrared cell using Tylan mass flow controllers. A stream of 0.5% CH<sub>3</sub>OH/He (99%) was delivered using a needle valve without further purification. Pressure in the cell was controlled using a back-pressure-regulator (Go).

In order to remove any residual surface species prior to testing, each sample was calcined in a 10% O<sub>2</sub>/He mixture flowing at 60 cm<sup>3</sup>/min. The sample was heated from room temperature to 523 K at 2 K/min and then maintained at 523 K for 8 h. Next, the sample was cooled to 323 K, swept with He, and reduced in a 10% H<sub>2</sub>/He mixture flowing at the rate of 60 cm<sup>3</sup>/min while the temperature was increased at the rate of 2 K/min up to 523 K. The flow of 10% H<sub>2</sub>/He was maintained at 523 K for 1 h prior to switching to a flow of 100% H<sub>2</sub> for an additional 1-3 h. The sample was then flushed with He for 1 h prior to initiating an experiment.

## **Results**

### *1.2 wt% Cu/t-ZrO<sub>2</sub>*

Figure 1 shows infrared spectra obtained during CO adsorption at 523 K on 1.2 wt% Cu/t-ZrO<sub>2</sub> exposed to a flow of 15% CO/He at a total pressure of 0.50 MPa. Strong

bands are observed at 1567, 1385, and 1367  $\text{cm}^{-1}$  attributable to the  $\nu_{\text{as}}(\text{OCO})$ ,  $\delta(\text{CH})$ , and  $\nu_{\text{s}}(\text{OCO})$  modes, respectively, of b-HCOO-Zr [9, 15, 16-22]. In the C-H stretching region, features at 2973 and 2892  $\text{cm}^{-1}$  become apparent after about 15 min and grow in intensity with time. The 2892  $\text{cm}^{-1}$  band is assigned to the C-H stretching vibration of b-HCOO-Zr [9, 15-21], while the 2973  $\text{cm}^{-1}$  band is attributed to a combination of the asymmetric O-C-O stretching and C-H bending modes of the same species [19, 20, 23]. Virtually identical spectra were obtained upon exposure of t-ZrO<sub>2</sub> in the absence of Cu, confirming that Cu does not influence the adsorption of CO as bidentate formate species on the surface of t-ZrO<sub>2</sub>.

Formate formation has been attributed to the interaction of CO with hydroxyl groups on ZrO<sub>2</sub> during CO adsorption [17, 25-28]. Evidence for this interaction is presented in Figure 2, which shows spectra obtained in the OH stretching region during the experiment presented in Figure 1. Bands appear at 3660 and 3738  $\text{cm}^{-1}$  due to Zr-OH groups on t-ZrO<sub>2</sub> [29, 30]. These bands are negative and increase in intensity with the duration of CO exposure, indicating that ZrOH groups are consumed upon the adsorption of CO.

After CO adsorption for 1 h, transient response spectra were recorded during CO hydrogenation at 523 K. H<sub>2</sub> was introduced into the flowing 15% CO/He (total pressure = 0.50 MPa) so as to achieve a H<sub>2</sub>/CO ratio of 3/1. Figure 3 shows that the features for b-HCOO-Zr (2973, 2894, 1565, 1384, and 1366  $\text{cm}^{-1}$ ) continue to increase in intensity up to about 4 h, at which time they approach a steady-state level. After about 4 min, bands at 2937 and 2837  $\text{cm}^{-1}$ , attributable to the  $\nu(\text{CH}_3)$  modes of CH<sub>3</sub>O-Zr [16, 17, 19, 29, 25, 31-33], become apparent. These bands increase in intensity, reaching a steady-state level

after approximately 4 h. A small band at approximately  $1474\text{ cm}^{-1}$  becomes apparent at longer times and is ascribed to the  $\delta(\text{CH})$  mode of  $\text{CH}_3\text{O-Zr}$  species [9, 20, 32].

### *1.2 wt% Cu/m-ZrO<sub>2</sub>*

Figure 4 shows infrared spectra recorded during CO adsorption on 1.2 wt% Cu/m-ZrO<sub>2</sub> at 523 K. The catalyst was exposed to a flow of 15% CO/He at a total pressure of 0.50 MPa. The features for b-HCOO-Zr (2969, 2883, 2748, 1563, 1386, and  $1366\text{ cm}^{-1}$ ) are significantly more intense than the analogous bands observed for 1.2 wt% Cu/t-ZrO<sub>2</sub>. The small band in the C-H stretching region at  $2745\text{ cm}^{-1}$  is ascribed to a combination of the  $\delta(\text{CH})$  and  $\nu_s(\text{OCO})$  modes of b-HCOO-Zr [20, 23]. Features attributable to  $\text{CH}_3\text{O-Zr}$  ( $2934$  and  $2830\text{ cm}^{-1}$ ) appear almost immediately, even in the absence of gas phase H<sub>2</sub>, and continue to increase in intensity for the duration of the experiment ( $\sim 1\text{ h}$ ). At the same time, bands appear at  $1039$  and  $1142\text{ cm}^{-1}$ , and increase in intensity at a rate similar to that for the bands at  $2936$  and  $2836\text{ cm}^{-1}$ . These peaks are assigned to the C-O stretch of terminal (t-OCH<sub>3</sub>) and bridged (b-OCH<sub>3</sub>) methoxide species on ZrO<sub>2</sub>, respectively [32, 34, 35]. The features at  $1034$  and  $1142\text{ cm}^{-1}$  were not observable with 1.2 wt% Cu/t-ZrO<sub>2</sub> due to strong sample absorptions below  $1200\text{ cm}^{-1}$ . The shoulder located at approximately  $1320\text{ cm}^{-1}$  is assigned to b-CO<sub>3</sub><sup>2-</sup>-Zr species [22, 25]. Similar spectra were recorded for m-ZrO<sub>2</sub> in the absence of Cu. The primary difference is that intensity of the bands for formate species in the spectra for 1.2 wt% Cu/m-ZrO<sub>2</sub> are less intense than those observed on m-ZrO<sub>2</sub>, due possibly to the hydrogenation of some of these species to methoxy groups in the former case. However, as with 1.2% Cu/t-ZrO<sub>2</sub>, all of the bands observed during the adsorption of CO on 1.2% Cu/m-ZrO<sub>2</sub> are ascribable to adsorption on ZrO<sub>2</sub>.

Figure 5 presents spectra obtained in the OH stretching region during the adsorption of CO on 1.2% Cu/m-ZrO<sub>2</sub>. Negative absorbance bands at 3730 and 3670 cm<sup>-1</sup> are ascribed to the consumption of Zr-OH groups on m-ZrO<sub>2</sub> [29, 30]. Consistent with the larger amount of formate species detected on 1.2 wt% Cu/m-ZrO<sub>2</sub>, a significantly greater decrease in Zr-OH was observed compared to that seen during CO adsorption on 1.2 wt% Cu/t-ZrO<sub>2</sub> (Fig. 2). 1.2 wt% Cu/m-ZrO<sub>2</sub> exhibits a larger consumption of lower frequency hydroxyl species relative to the higher frequency hydroxyl species, opposite to that observed on 1.2 wt% Cu/t-ZrO<sub>2</sub>. This observation suggests that the Zr-OH groups responsible for the band at 3670 cm<sup>-1</sup> are consumed by reaction with CO more slowly than those at 3730 cm<sup>-1</sup>.

Figure 6 shows transient-response spectra obtained during CO hydrogenation on 1.2 wt% Cu/m-ZrO<sub>2</sub> at 523 K. Spectra were obtained by introducing H<sub>2</sub> into the flowing 15% CO/He (total pressure = 0.50 MPa) so as to achieve a H<sub>2</sub>/CO ratio of 3/1. The features for b-HCOO-Zr at 1564, 1385, and 1367 cm<sup>-1</sup> decrease in intensity rapidly as soon as H<sub>2</sub> is introduced while, concurrently, peaks for CH<sub>3</sub>O-Zr at 1039 and 1142 cm<sup>-1</sup> increase in intensity rapidly. In the C-H stretching region, the bands for CH<sub>3</sub>O-Zr are particularly intense and increase in intensity until they reach a steady-state level after approximately 80 min. The corresponding C-O stretching bands (1039 and 1142 cm<sup>-1</sup>) increase in a similar manner. As adsorption progresses each C-H stretch red shifts approximately 10-15 cm<sup>-1</sup> while each of the C-O stretches blue shift approximately 3-8 cm<sup>-1</sup>, due possibly to interactions between surface species as surface coverage increases. The  $\delta(\text{CH})$  feature for CH<sub>3</sub>O-Zr (1446 cm<sup>-1</sup>) is evident initially but remains relatively small throughout the transient. Comparison of Figs. 4 and 6 shows that the intensities of

the bands for CH<sub>3</sub>O-Zr are approximately an order of magnitude larger on 1.2wt% Cu/m-ZrO<sub>2</sub> than on 1.2wt% Cu/t-ZrO<sub>2</sub>.

#### *Transient-Response Experiments*

The temporal evolution of the principle surface species on 1.2% Cu/t-ZrO<sub>2</sub> and 1.2% Cu/m-ZrO<sub>2</sub> during the CO hydrogenation are compared in Figure 7. The band at 1564(5) cm<sup>-1</sup> was used to follow the dynamics of b-HCOO-Zr and the band at either 2837 cm<sup>-1</sup> or 2821 cm<sup>-1</sup> was used to follow the dynamics of CH<sub>3</sub>O-Zr. The peak areas for both b-HCOO-Zr and CH<sub>3</sub>O-Zr were normalized to the value observed after approximately 12 h of exposure to CO/H<sub>2</sub>. For 1.2 wt% Cu/t-ZrO<sub>2</sub> the concentration of b-HCOO-Zr continues to rise following 1 h of CO adsorption (represented by time 0 in Figure 7). By contrast, the concentration of formate species on 1.2 wt% Cu/m-ZrO<sub>2</sub> undergoes a rapid initial decrease relative to the level observed in the absence of gas phase H<sub>2</sub>, before decreasing more slowly over the remainder of the transient.

The intensity of the band for CH<sub>3</sub>O-Zr increases with the time of catalyst exposure to the CO/H<sub>2</sub> mixture, but the dynamics of band growth are quite different for 1.2% Cu/t-ZrO<sub>2</sub> and 1.2% Cu/m-ZrO<sub>2</sub>. For 1.2 wt% Cu/m-ZrO<sub>2</sub> the intensity of the CH<sub>3</sub>O-Zr band increases very rapidly over the initial 25 min and then approaches a plateau after about 1 h. The dynamics of this feature are very similar to those for the band associated with b-HCOO-Zr, but opposite in direction, suggesting that on 1.2% Cu/m-ZrO<sub>2</sub> b-HCOO-Zr undergoes rapid hydrogenation to CH<sub>3</sub>O-Zr. By contrast, the intensity of the HCOO-Zr band on 1.2 wt% Cu/t-ZrO<sub>2</sub> increases with time, suggesting a slower conversion of formate to methoxide species.

The rate at which surface species are consumed was probed by removing CO from the feed at the conclusion of the CO hydrogenation experiments shown in Figures 3 and 6. Figure 8 compares the dynamics of b-HCOO-Zr and CH<sub>3</sub>O-Zr consumption on 1.2% Cu/t-ZrO<sub>2</sub> and 1.2% Cu/m-ZrO<sub>2</sub>. Transient-response spectra were obtained by replacing the flow of 15% CO/He in the flow used for CO hydrogenation by an equivalent flow of pure He, while maintaining a constant H<sub>2</sub> partial pressure of 0.15 MPa. The intensity of the band for b-HCOO-Zr decreases monotonically for both catalysts, but much more rapidly for 1.2% Cu/m-ZrO<sub>2</sub>. The intensity of the band for CH<sub>3</sub>O-Zr also undergoes a monotonic decrease for both catalysts, but the rate of decrease is significantly slower than that for b-HCOO-Zr. Figure 8c shows that immediately upon cessation of the flow of CO there is a short period during which the surface concentration of CH<sub>3</sub>O-Zr remains relatively constant before it begins to decline. This observation suggests that formate species undergo rapid hydrogenation to methoxide species on both phases of ZrO<sub>2</sub>, but that the reductive elimination of methoxide species occurs at a slower rate. Figures 8b and 8c show that the rate of removal of CH<sub>3</sub>O-Zr is initially more rapid on 1.2% Cu/m-ZrO<sub>2</sub> than 1.2% Cu/t-ZrO<sub>2</sub>, but that for longer times the relative rates become comparable.

#### *Effect of Cu Loading on Cu/m-ZrO<sub>2</sub>*

The results presented in the Part I of this study demonstrated that Cu/m-ZrO<sub>2</sub> exhibits a higher steady-state methanol synthesis activity than Cu/t-ZrO<sub>2</sub> (see Table 1). Increasing the Cu surface density on m-ZrO<sub>2</sub> further improves the activity. Experiments were carried out to investigate the effects of Cu loading on the dynamics of species formation and consumption. Figure 9 shows spectra of Cu/m-ZrO<sub>2</sub> catalysts taken after 6

h of CO hydrogenation at 523 K with a 3/1 H<sub>2</sub>/CO ratio and a total pressure of 0.50 MPa. Comparison of these spectra reveals that while the intensity of the bands for b-HCOO-Zr are relatively independent of Cu loading and Cu surface coverage, the intensity of the bands for CH<sub>3</sub>O-Zr increase with Cu surface coverage (Table 2).

A comparison of the temporal evolution of b-HCOO-Zr and CH<sub>3</sub>O-Zr during the onset of CO hydrogenation after CO adsorption for 1 h over each catalyst is given in Figure 10. Peak areas for both b-HCOO-Zr and CH<sub>3</sub>O-Zr have been normalized to the value observed after reaction for approximately 12 h. The dynamics of b-HCOO-Zr consumption are independent of Cu loading. Initially, the surface concentration of b-HCOO-Zr decreases rapidly from the level observed prior to the introduction of H<sub>2</sub>, after which it declines more slowly over the remainder of the transient. Although the absolute concentration of CH<sub>3</sub>O-Zr varies amongst Cu/m-ZrO<sub>2</sub> catalysts, the relative dynamics of CH<sub>3</sub>O-Zr formation are also virtually independent of Cu loading. The time scale of the rise in the concentration of CH<sub>3</sub>O-Zr closely parallels the pattern of decrease in the surface concentration of b-HCOO-Zr.

The relative rate of consumption of surface species was examined by replacing the flow of CO used for CO hydrogenation by an equivalent flow of He while maintaining the H<sub>2</sub> partial pressure. Figure 11 compares the dynamics of b-HCOO-Zr and CH<sub>3</sub>O-Zr consumption for each of the Cu/m-ZrO<sub>2</sub> catalysts. Peak areas for both b-HCOO-Zr and CH<sub>3</sub>O-Zr are normalized to the value observed at the beginning of the transient. The initial rate of consumption of b-HCOO-Zr is independent of Cu loading. After approximately 20 min, though, the rate of b-HCOO-Zr consumption from the higher weight-loaded materials decreases significantly. This suggests the possible

existence of two distinct formate species present on the surface of m-ZrO<sub>2</sub>. A similar distinction has been reported with formate species formed on ZnO in studies of CO hydrogenation on Cu/ZnO/Al<sub>2</sub>O<sub>3</sub> [36]. In contrast to the removal of b-HCOO-Zr, a significantly greater portion of methoxide species were removed from the surface of the catalyst having a Cu weight loading higher than 1.2 wt%. The apparent first-order rate constant for the removal of methoxide species determined from the initial portion of the transient is given in Table 2. The decrease over the course of the experiment was approximately equivalent for 6.4, 10, and 20 wt% Cu/m-ZrO<sub>2</sub>. Given that b-HCOO-Zr is a precursor to CH<sub>3</sub>O-Zr on the surface, it is unclear whether the slower relative decrease of methoxide species on 1.2 wt% Cu/m-ZrO<sub>2</sub> is a reflection of a higher rate of methoxide group formation through the hydrogenation of b-HCOO-Zr or an inherent difference in the ability to reductively eliminate CH<sub>3</sub>O-Zr on the surface.

To isolate the inherent dynamics of reductive elimination, CH<sub>3</sub>OH was dosed onto both 1.2 wt% Cu/m-ZrO<sub>2</sub> and 10 wt% Cu/m-ZrO<sub>2</sub> at 523 K. In each case, the catalyst was exposed to a flow containing 0.5% CH<sub>3</sub>OH/He for 1 h at a total pressure of 0.50 MPa. This process produced CH<sub>3</sub>O-Zr bands identical to those observed during CO hydrogenation over both catalysts. The CH<sub>3</sub>O-Zr species produced in this fashion were then exposed to flowing H<sub>2</sub> in a manner identical to that used for the experiments presented in Figure 11. Figure 12 shows the dynamics of consumption of CH<sub>3</sub>O-Zr. Peak areas for CH<sub>3</sub>O-Zr were normalized to the value observed at the beginning of the transient after the removal of physisorbed species (~ 2 min). For both catalysts the rate of CH<sub>3</sub>O-Zr hydrogenation is equivalent to that observed following CO hydrogenation

(see Figure 11), with the rate of CH<sub>3</sub>O-Zr hydrogenation higher on 10% Cu/m-ZrO<sub>2</sub> than on 1.2% Cu/m-ZrO<sub>2</sub>.

The rate of CH<sub>3</sub>O-Zr elimination is limited by the concentration of H atoms on the surface of ZrO<sub>2</sub>, which in turn is limited by the supply of H atoms provided by spillover from Cu. Consistent with this reasoning, it is observed that in the absence of Cu, the rate of CH<sub>3</sub>O-Zr hydrogenation is an order of magnitude slower than that observed on 1.2% Cu/m-ZrO<sub>2</sub>. As the surface concentration of Cu is raised, the surface concentration of H atoms increases up to the point at which it reaches equilibrium with respect to the gas phase partial pressure of H<sub>2</sub>. When equilibrium is achieved, the rates of H-atom spillover from Cu and reverse spillover back to Cu become identical. The absence of a dependence of the rate of CH<sub>3</sub>O-Zr hydrogenation on Cu for Cu surface concentration of 1.88 m<sup>2</sup>/g suggests that at such Cu surface concentrations, the H-atom concentration on the surface of m-ZrO<sub>2</sub> has reached equilibrium with the gas phase.

## Discussion

Previous studies suggest that the mechanism of CO hydrogenation over Cu/ZrO<sub>2</sub> catalysts can be described in terms of the following sequence of reactions [9, 12].

1.  $\text{CO}_g + (\text{Zr})_2\text{OH} \leftrightarrow \text{b-HCOOZr} + \text{Zr}$
2.  $\text{b-HCOOZr} + \text{H}_s \rightarrow \dots \rightarrow \text{CH}_3\text{O-Zr} + \text{Zr-OH}$
3.  $\text{CH}_3\text{O-Zr} + \text{H}_s \rightarrow \rightarrow \text{CH}_3\text{OH} + (\text{Zr})_2\text{OH}$

(Zr)<sub>2</sub>OH represents a hydroxyl group adjacent to coordinatively unsaturated Zr cation produced upon creation of an anionic vacancy at the surface of ZrO<sub>2</sub> (see Figure 12 in Ref. [12]). CO is adsorbed reversibly in reaction 1 to form a bidentate formate species

(b-HCOOZr). This species then reacts with H atoms present on the surface of ZrO<sub>2</sub>, (H<sub>s</sub>), ultimately forming methoxide species (CH<sub>3</sub>O-Zr) via reaction 2. The reductive elimination of methoxide species in reaction 3 leads to the formation of methanol. Reactions 2 and 3 are taken to be irreversible, since under the reaction conditions used in this study no evidence was found for the dehydrogenation of methoxide or formate species.

As noted earlier, H<sub>s</sub> is provided by spillover of H atoms from the dispersed Cu, which adsorbs H<sub>2</sub> dissociatively. Investigations of the rate of H/D exchange into hydroxyl groups present on the surface of ZrO<sub>2</sub> indicate that at reaction temperature the rate of H atom spillover is about an order of magnitude more rapid than the rate of CO hydrogenation and is significantly faster on Cu/m-ZrO<sub>2</sub> than Cu/t-ZrO<sub>2</sub> [11, 37]. Studies of methanol decomposition to H<sub>2</sub> and CO<sub>2</sub> indicate that the decomposition of methanol proceeds on ZrO<sub>2</sub> and that dispersed Cu is necessary to facilitate the recombination of H atoms [38]. Taken together, these observations suggest during CO hydrogenation to methanol, the steady-state inventory of H atoms on the surface of ZrO<sub>2</sub> is determined by the rates of forward and reverse H-atom spillover and the rate of H-atom consumption for CO hydrogenation. When the rate of CO hydrogenation is slow relative to the rates of forward and reverse spillover, then the concentration of H<sub>s</sub> will reach an equilibrium level.

The effects of ZrO<sub>2</sub> phase on the hydrogenation of CO over 1.2% Cu/t-ZrO<sub>2</sub> and 1.2% Cu/m-ZrO<sub>2</sub> can now be interpreted in terms of the relative rates of individual steps in the above scheme. Figure 7 shows that the adsorption of CO on 1.2% Cu/t-ZrO<sub>2</sub> is slow, and continues to occur over 6 h, even after H<sub>2</sub> has been added to the flow of CO

and the hydrogenation of CO has begun. This suggests that the apparent first-order rate coefficient for reaction 1 is faster than that for reaction 2. By contrast, the rate of CO adsorption on 1.2% Cu/m-ZrO<sub>2</sub> is very rapid, and the surface of the catalyst becomes saturated with CO within approximately 1 h (see Figure 4). When H<sub>2</sub> is added to the flow of CO over this catalyst, the surface concentration of b-HCOOZr species decreases rapidly and the surface concentration of CH<sub>3</sub>O-Zr species increases at the same rate, as seen in Figure 7. This pattern suggests that the apparent first-order rate coefficient for reaction 2 is faster than that for the reverse of reaction 1. It is also evident from Figure 7 that the apparent first order rate coefficient for the formation of CH<sub>3</sub>O-Zr, determined from the initial slopes of the curves, is a factor of about 2.5 faster for 1.2% Cu/m-ZrO<sub>2</sub> than 1.2% Cu/t-ZrO<sub>2</sub>. A very similar ratio in apparent first-order rate coefficients is seen in Figure 8 for the reductive elimination of CH<sub>3</sub>O-Zr as methanol. If it is assumed that the intrinsic rate coefficient for hydrogenation of b-HCOOZr and CH<sub>3</sub>O-Zr are independent of the phase of ZrO<sub>2</sub>, then the ratio of apparent rate coefficients suggests that the concentration of H<sub>s</sub> is ~ 2.5 fold greater on 1.2% Cu/m-ZrO<sub>2</sub>. A higher concentration of H<sub>s</sub> on Cu/m-ZrO<sub>2</sub> relative to Cu/t-ZrO<sub>2</sub> would follow from the observation of a higher rate of H-atom spillover (as well as for reverse spillover presumably) for the former catalyst, as noted above.

The order of magnitude higher rate of methanol synthesis over 1.2% Cu/m-ZrO<sub>2</sub> relative to 1.2% Cu/t-ZrO<sub>2</sub> can be explained in the following manner. We note first that concentration of all carbon-containing species on the former catalyst is higher. Comparison of Figures 3 and 6 shows that after 6 h of reaction, the surface concentration of b-HCOOZr is ~ 3 times higher on 1.2% Cu/m-ZrO<sub>2</sub> than 1.2% Cu/t-ZrO<sub>2</sub>, and more

importantly, the surface concentration of  $\text{CH}_3\text{O-Zr}$  is  $\sim 14$  times higher on 1.2% Cu/m- $\text{ZrO}_2$ . Since the reductive elimination of  $\text{CH}_3\text{O-Zr}$  is irreversible under the conditions of the experiments reported here, its rate is equivalent to the rate of methanol synthesis. A similar conclusion was reached in an earlier study by following simultaneously the appearance of the infrared band for  $\text{CH}_3\text{O-Zr}$  and the appearance of methanol in the gas phase [9]. Thus one can estimate the relative rates of methanol synthesis on 1.2% Cu/t- $\text{ZrO}_2$  and 1.2% Cu/m- $\text{ZrO}_2$  by taking the product of the apparent rate coefficient for the reductive elimination of  $\text{CH}_3\text{O-Zr}$  and the surface concentration of this species as measured by the intensity of its infrared band (see Table 3). Based on this analysis it is concluded that the rate of methanol synthesis on 1.2% Cu/m- $\text{ZrO}_2$  should be 34 times higher than that on 1.2% Cu/t- $\text{ZrO}_2$ . While this factor is greater than the observed 8-fold higher steady-state methanol synthesis activity of 1.2% Cu/m- $\text{ZrO}_2$  over 1.2%Cu/t- $\text{ZrO}_2$ , it supports the idea that the higher rate of methanol synthesis on 1.2% Cu/m- $\text{ZrO}_2$  is due largely to the higher concentration of anionic vacancies on the surface of m- $\text{ZrO}_2$ . These sites facilitate the rapid adsorption of CO.

In Part I of this study it was shown that the methanol synthesis activity of Cu/m- $\text{ZrO}_2$  catalysts is proportional to the surface area of exposed Cu atoms (see also Table 1). To interpret this observation, it is necessary to consider what happens as the surface concentration of Cu is increased. Table 2 lists the surface concentration of  $\text{CH}_3\text{O-Zr}$  and the values of the apparent rate coefficient,  $k_{\text{app}}$ , for the reductive elimination of methoxide groups from the surface of m- $\text{ZrO}_2$  as a function of Cu surface area. It is evident that the surface concentration of  $\text{CH}_3\text{O-Zr}$  increases with the surface area of Cu up to the level of  $\sim 2.5 \text{ m}^2/\text{g}$ , whereupon the concentration of  $\text{CH}_3\text{O-Zr}$  appears to become constant. The

observed variation in the concentration of CH<sub>3</sub>O-Zr groups is dictated by the balance between the formation and consumption of these species. Since the surface concentration of b-HCOOZr species is essentially independent of the Cu surface area, the increase in the surface concentration of CH<sub>3</sub>O-Zr is attributed to a higher surface concentration of H<sub>s</sub>. If it is assumed that Reaction 2 is near equilibrium, then one would expect the surface concentration of ZrOCH<sub>3</sub> to rise as the surface concentration of H<sub>s</sub> increases. The plateau in the surface concentration of ZrOCH<sub>3</sub> is attributed to saturation of the ZrO<sub>2</sub> surface by H<sub>s</sub> when the surface area of Cu is greater than ~2.5 m<sup>2</sup>/g. Table 2 shows that the value of k<sub>app</sub> also with increasing Cu surface area but reaches an apparent plateau above a Cu surface area of ~1.9 m<sup>2</sup>/g. Since k<sub>app</sub> is the product of the intrinsic rate coefficient for Reaction 3 and the surface coverage by H<sub>s</sub>, the approach of k<sub>app</sub> to a plateau is taken to coincide roughly with the approach of the coverage of H<sub>s</sub> to equilibrium. The anticipated effect of Cu surface area on the rate of methanol synthesis can be estimated by taking the product of the surface coverage of CH<sub>3</sub>O-Zr and k<sub>app</sub>. As seen in Figure 13, this leads to a linear relationship, which passes through the origin, in good agreement with what is observed from measurements of the rate of methanol synthesis at steady state (see Table 1) [12].

## Conclusions

Formate and methoxide species bound to zirconia are detected by *in situ* infrared spectroscopy on the surfaces of Cu/t-ZrO<sub>2</sub> and Cu/m-ZrO<sub>2</sub> during methanol synthesis from CO and H<sub>2</sub>. The surface concentrations of both species on are an order of magnitude smaller on Cu/t-ZrO<sub>2</sub> than on Cu/m-ZrO<sub>2</sub>. Transient-response experiments

suggest that for both catalysts the rate-limiting step in the synthesis of methanol from CO is the reductive elimination of  $\text{CH}_3\text{O-Zr}$  species present on the surface of zirconia. The apparent first-order rate coefficient for this process is about 2.5 times higher for Cu/m- $\text{ZrO}_2$  than for Cu/t- $\text{ZrO}_2$ . A major part of this difference is believed to be due to the higher surface concentration of atomic hydrogen on the surface of m- $\text{ZrO}_2$  than t- $\text{ZrO}_2$ . It is estimated from the product of the coverage of  $\text{ZrOCH}_3$  and  $k_{\text{app}}$  that the rate of methanol synthesis should be more than an order of magnitude higher on Cu/m- $\text{ZrO}_2$  than on Cu/t- $\text{ZrO}_2$ , in good qualitative agreement with experimental observation. Both  $k_{\text{app}}$  and the surface concentration of  $\text{CH}_3\text{O-Zr}$  increase with increasing Cu surface area, but reach a plateau. The plateau in each case is attributed to the attainment of an equilibrium concentration in the coverage of the zirconia surface by adsorbed H atoms. The rate of methanol synthesis estimated from the product of  $k_{\text{app}}$  and the surface coverage of  $\text{CH}_3\text{O-Zr}$  versus the Cu surface area yields a linear relationship, in good agreement with the relationship seen between the steady-state rate of methanol synthesis and the Cu surface area.

### **Acknowledgement**

This work was supported by the Director, Office of Basic Energy Sciences, Chemical Sciences Division of the U.S. Department of Energy under Contract DE-AC03-76SF00098.

## References

1. Denise, B., and Sneed, R.P.A., *Appl. Catal.* **28**, 235 (1986).
2. Amenomiya, Y., *Appl. Catal.* **30**, 57 (1987).
3. Nitta, Y., Fujimatsu, T., Okamoto, Y., and Imanaka, T., *Catal. Lett.* **17**, 157 (1993).
4. Sun, Y., and Sermon, P.A., *J. Chem. Soc. Commun.* 1242 (1993).
5. Bianchi, D., Gass, J.L., Khalfallah, M., and Teichner, S.J., *Appl. Catal.* **101**, 297 (1993).
6. Nitta, Y., Suwata, O., Ikeda, Y., Okamoto, Y., and Imanaka, T., *Catal. Lett.* **26**, 345 (1994).
7. Sun, Y., and Sermon, P.A., *Catal. Lett.* **29**, 361 (1994).
8. Fisher, I.A., Woo, H.C., and Bell, A.T., *Catal. Lett.* **44**, 11 (1997).
9. Fisher, I.A., and Bell, A.T., *J. Catal.* **172**, 222 (1997); *J. Catal.* **178**, 153 (1998).
10. Wambach, J., Baiker, A., and Wokaun, A., *Phys. Chem. Chem. Phys.* **1**, 5071 (1999).
11. Jung, K. T., and Bell, A. T., *Catal. Lett.* **80**, 63 (2002).
12. Rhodes, M. J., and Bell, A. T., *J. Catal.*, submitted.
13. Sato, S., Takahashi, R., Sodesawa, T., Yuma, K., and Obata, Y., *J. Catal.* **196**, 195 (2000).
14. Hicks, R.F., Kellner, C.S., Savatsky, B.J., Hecker, W.C., and Bell, A.T., *J. Catal.* **71**, 216 (1981).
15. Schild, C., Wokaun, A., and Baiker, A., *J. Mol. Catal.* **63**, 243 (1990).
16. He, M.Y., and Ekerdt, J.G., *J. Catal.* **87**, 381 (1984).

17. Kondo, J., Abe, H., Sakata, Y., Maruya, K., Domen, K., and Onishi, T., *J. Chem. Soc., Faraday Trans. 1* **84**, 511 (1988).
18. Hertl, W., *Langmuir* **5**, 96 (1989).
19. Guglielminotti, E., *Langmuir* **6**, 1455 (1990).
20. Bianchi, D., Chafik, T., Khalfallah, M., and Teichner, S.J., *Appl. Catal. A: Gen.* **105**, 223 (1993).
21. Kalies, H., Pinto, N., Pajonk, G.M., and Bianchi, D., *Appl. Catal. A: Gen.* **202**, 197 (2000).
22. Pokrovski, K., Jung, K.T., and Bell, A.T., *Langmuir* **17**, 4297 (2001).
23. Edwards, J., and Schrader, G., *J. Phys. Chem.* **89**, 782 (1985).
24. Bianchi, D., Chafik, T., Khalfallah, M., and Teichner, S.J., *Appl. Catal. A: Gen.* **112**, 57 (1994).
25. Jung, K.D., and Bell, A.T., *J. Catal.* **193**, 207 (2000).
26. Okamoto, Y., and Gotoh, H., *Catal. Today* **36**, 71 (1997).
27. Okamoto, Y., Gotoh, H., Aritani, H., Tanaka, T., and Yoshida, S., *J. Chem. Soc., Faraday Trans.* **93**, 3879 (1997).
28. Indovina, V., Occhiuzzi, M., Pietrogiacomini, D., and Tuti, S., *J. Phys. Chem. B* **103**, 9967 (1999).
29. Erkelens, J., Rijnten, H.Th., and Eggink-Du Burck, S.H., *Recueil* **91**, 1426 (1972).
30. Trunschke, A., Hoang, D.L., and Lieske, H., *J. Chem. Soc., Faraday Trans.* **91**, 4441 (1995).
31. Weigel, J., Koepfel, R.A., Baiker, A., and Wokaun, A., *Langmuir* **12**, 5319 (1996).

32. Bensitel, M., Moravek, V., Lamonte, J., Saur, O., and Lavalley, J.C., *Spectrochimica Acta.* **43a**, 1487 (1987).
33. Bianchi, D., Chafik, T., Khalfallah, M., and Teichner, S.J., *Appl. Catal. A: Gen.* **123**, 89 (1995).
34. Ouyang, F., Kondo, J.N., Maruya, K., and Domen, K., *J. Phys. Chem. B* **101**, 4867 (1997).
35. Ouyang, F., Kondo, J.N., Maruya, K., and Domen, K., *Catal. Lett.* **50**, 179 (1998).
36. Saussey, J., and Lavalley, J.C., *J. Mol. Catal.* **50**, 343 (1989).
37. Jung, K. D., and Bell, J. Catal. **193**, 207 (2000).

**Table 1.** Surface area and methanol synthesis activity for Cu/t-ZrO<sub>2</sub> and Cu/m-ZrO<sub>2</sub>.  
Reaction Conditions: T = 523 K; P = 3.0 MPa; H<sub>2</sub>/CO = 3; total flow rate = 60 cm<sup>3</sup>/min.

Sample	Cu Surface Area (m <sup>2</sup> /g)	Mass Specific Rate (μmol/g <sub>cat</sub> ·s)
1.2 wt% Cu/t-ZrO <sub>2</sub>	1.44	0.14
1.2 wt% Cu/m-ZrO <sub>2</sub>	0.87	1.1
6.4 wt% Cu/m-ZrO <sub>2</sub>	2.46	2.7
10 wt % Cu/m-ZrO <sub>2</sub>	2.70	3.0
20 wt% Cu/m-ZrO <sub>2</sub>	1.88	1.5

**Table 2.** Steady-state peak areas of CH<sub>3</sub>O-Zr and apparent first-order rate coefficients for the removal of CH<sub>3</sub>O-Zr from 1.2, 6.4, 10, and 20 wt% Cu/m-ZrO<sub>2</sub>.

Sample	k <sub>app</sub> (min <sup>-1</sup> )	θ <sub>CH<sub>3</sub>O</sub> (a.u.)
1.2 wt% Cu/m-ZrO <sub>2</sub>	4.1×10 <sup>-3</sup>	12.9
6.4 wt% Cu/m-ZrO <sub>2</sub>	8.2×10 <sup>-3</sup>	21.3
10 wt % Cu/m-ZrO <sub>2</sub>	7.7×10 <sup>-3</sup>	21.6
20 wt% Cu/m-ZrO <sub>2</sub>	7.6×10 <sup>-3</sup>	16.5

**Table 3.** Steady-state peak areas of CH<sub>3</sub>O-Zr and apparent first-order rate coefficients for the removal of CH<sub>3</sub>O-Zr from 1.2 wt% Cu/t-ZrO<sub>2</sub> and 1.2 wt% Cu/m-ZrO<sub>2</sub>.

Sample	k <sub>app</sub> (min <sup>-1</sup> )	θ <sub>CH<sub>3</sub>O</sub> (a.u.)
1.2 wt% Cu/t-ZrO <sub>2</sub>	1.7×10 <sup>-3</sup>	0.9
1.2 wt% Cu/m-ZrO <sub>2</sub>	4.1×10 <sup>-3</sup>	12.9

## Figure Captions

- Fig. 1. Infrared spectra (C-H and C-O stretching regions) taken for 1.2 wt% Cu/t-ZrO<sub>2</sub> at 523 K after switching feed from 0.50 MPa He to 0.05 MPa CO and 0.45 MPa He flowing at a total rate of 60 cm<sup>3</sup>/min. Spectra referenced to 1.2 wt% Cu/t-ZrO<sub>2</sub> under 0.50 MPa He flow at 523 K.
- Fig. 2. Infrared spectra (O-H stretching region) taken for 1.2 wt% Cu/t-ZrO<sub>2</sub> at 523 K after switching feed from 0.50 MPa He to 0.05 MPa CO and 0.45 MPa He flowing at a total rate of 60 cm<sup>3</sup>/min. Spectra referenced to 1.2 wt% Cu/t-ZrO<sub>2</sub> under 0.50 MPa He flow at 523 K.
- Fig. 3. Infrared spectra taken for 1.2 wt% Cu/t-ZrO<sub>2</sub> at 523 K after switching feed from 0.05 MPa CO and 0.45 MPa He to 0.05 MPa CO, 0.15 MPa H<sub>2</sub>, and 0.30 MPa He flowing at a total rate of 60 cm<sup>3</sup>/min. Spectra referenced to 1.2 wt% Cu/t-ZrO<sub>2</sub> under 0.50 MPa He flow at 523 K.
- Fig. 4. Infrared spectra (C-H and C-O stretching regions) taken for 1.2 wt% Cu/m-ZrO<sub>2</sub> at 523 K after switching feed from 0.50 MPa He to 0.05 MPa CO and 0.45 MPa He flowing at a total rate of 60 cm<sup>3</sup>/min. Spectra referenced to 1.2 wt% Cu/m-ZrO<sub>2</sub> under 0.50 MPa He flow at 523 K.
- Fig. 5. Infrared spectra (O-H stretching region) taken for 1.2 wt% Cu/m-ZrO<sub>2</sub> at 523 K after switching feed from 0.50 MPa He to 0.05 MPa CO and 0.45 MPa He flowing at a total rate of 60 cm<sup>3</sup>/min. Spectra referenced to 1.2 wt% Cu/m-ZrO<sub>2</sub> under 0.50 MPa He flow at 523 K.
- Fig. 6. Infrared spectra taken for 1.2 wt% Cu/m-ZrO<sub>2</sub> at 523 K after switching feed from 0.05 MPa CO and 0.45 MPa He to 0.05 MPa CO, 0.15 MPa H<sub>2</sub>, and 0.30 MPa He flowing at a total rate of 60 cm<sup>3</sup>/min. Spectra referenced to 1.2 wt% Cu/m-ZrO<sub>2</sub> under 0.50 MPa He flow at 523 K.
- Fig. 7. Relative IR peak intensities versus time for (a) b-HCOO-Zr and (b) CH<sub>3</sub>O-Zr observed for 1.2 wt% Cu/t-ZrO<sub>2</sub> and 1.2 wt% Cu/m-ZrO<sub>2</sub> during the experiments shown in Figs. 3 and 6. Areas normalized to the values observed at the end of the transient.
- Fig. 8. Relative IR peak intensities versus time for (a) b-HCOO-Zr, (b) CH<sub>3</sub>O-Zr, and (c) initial 20 min of (b) observed for 1.2 wt% Cu/t-ZrO<sub>2</sub>, and 1.2 wt% Cu/m-ZrO<sub>2</sub> at 523 K after switching feed from 0.05 MPa CO, 0.15 MPa H<sub>2</sub>, and 0.30 MPa He to 0.15 MPa H<sub>2</sub> and 0.35 MPa He flowing at a total rate of 60 cm<sup>3</sup>/min. Areas normalized to the values observed at the beginning of the transient.
- Fig. 9. Infrared spectra taken for 1.2, 6.4, 10, and 20 wt% Cu/m-ZrO<sub>2</sub> at 523 K after switching feed from 0.05 MPa CO to 0.45 MPa He to 0.05 MPa CO, 0.15 MPa H<sub>2</sub>, and 0.30 MPa He flowing at a total rate of 60 cm<sup>3</sup>/min. Spectra referenced

to 1.2, 6.4, 10, and 20 wt% Cu/m-ZrO<sub>2</sub> under 0.50 MPa He flow at 523 K, respectively.

- Fig. 10. Relative IR peak intensities of (a) b-HCOO-Zr and (b) CH<sub>3</sub>O-Zr features for 0, 1.2, 6.4, 10, and 20 wt% Cu/m-ZrO<sub>2</sub> during the experiments in Fig. 9. Areas normalized to the values observed at the end of the transient.
- Fig. 11. Relative IR peak intensities of (a) b-HCOO-Zr, (b) CH<sub>3</sub>O-Zr, and (c) initial 20 min of (b) features for 0, 1.2, 6.4, 10, and 20 wt% Cu/m-ZrO<sub>2</sub> at 523 K after switching feed from 0.05 MPa CO, 0.15 MPa H<sub>2</sub>, and 0.30 MPa He to 0.15 MPa H<sub>2</sub> and 0.35 MPa He flowing at a total rate of 60 cm<sup>3</sup>/min. Areas normalized to the values observed at the beginning of the transient.
- Fig. 12. Relative IR peak intensities of CH<sub>3</sub>O-Zr features for 1.2 and 10 wt% Cu/m-ZrO<sub>2</sub> at 523 K after switching feed from 0.0025 MPa CH<sub>3</sub>OH and 0.4975 MPa He to 0.15 MPa H<sub>2</sub> and 0.35 MPa He flowing at a total rate of 60 cm<sup>3</sup>/min. Areas normalized to the values observed at the beginning of the transient.
- Fig. 13. Product of apparent first-order rate coefficient for CH<sub>3</sub>O-Zr removal and CH<sub>3</sub>O-Zr peak area versus Cu surface area for Cu/m-ZrO<sub>2</sub> catalysts.

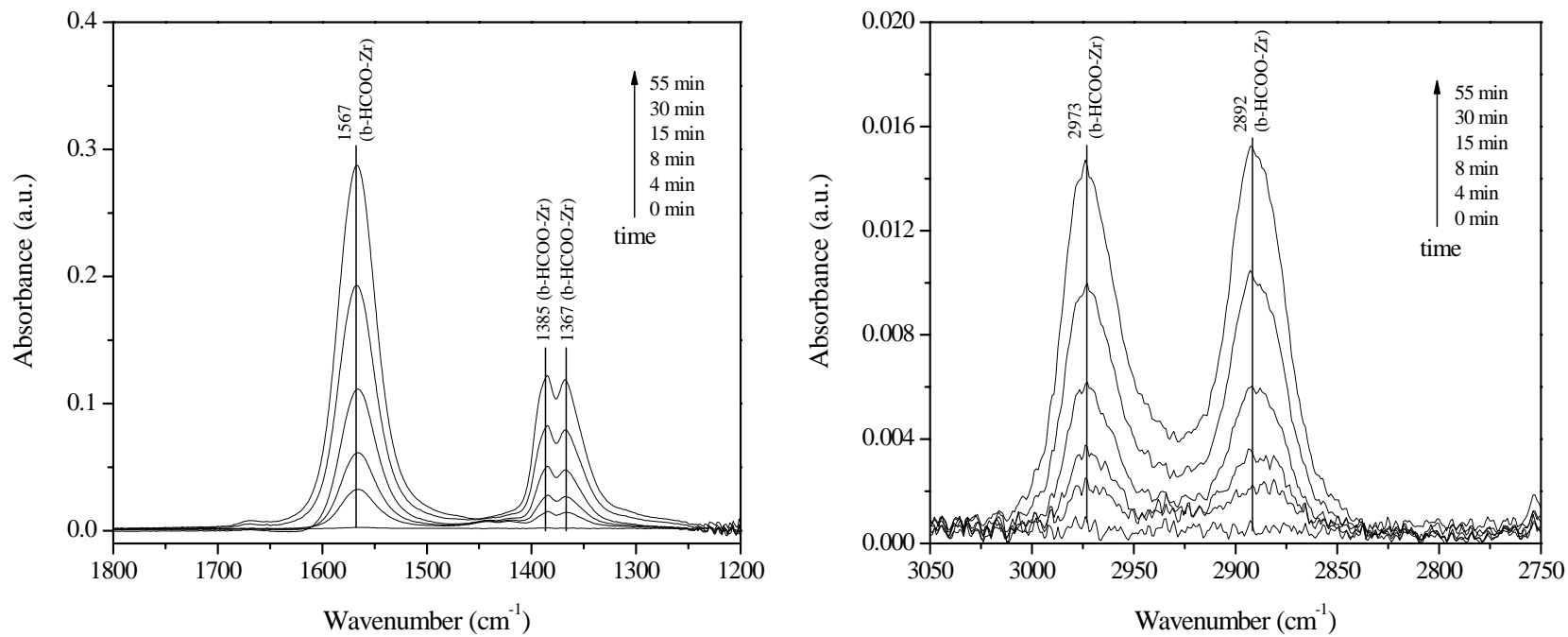


**Figure 1.** Infrared spectra (C-H and C-O stretching regions) taken for 1.2 wt% Cu/t-ZrO<sub>2</sub> at 523 K after switching feed from 0.50 MPa He to 0.05 MPa CO and 0.45 MPa He flowing at a total rate of 60 cm<sup>3</sup>/min. Spectra referenced to 1.2 wt% Cu/t-ZrO<sub>2</sub> under 0.50 MPa He flow at 523 K.

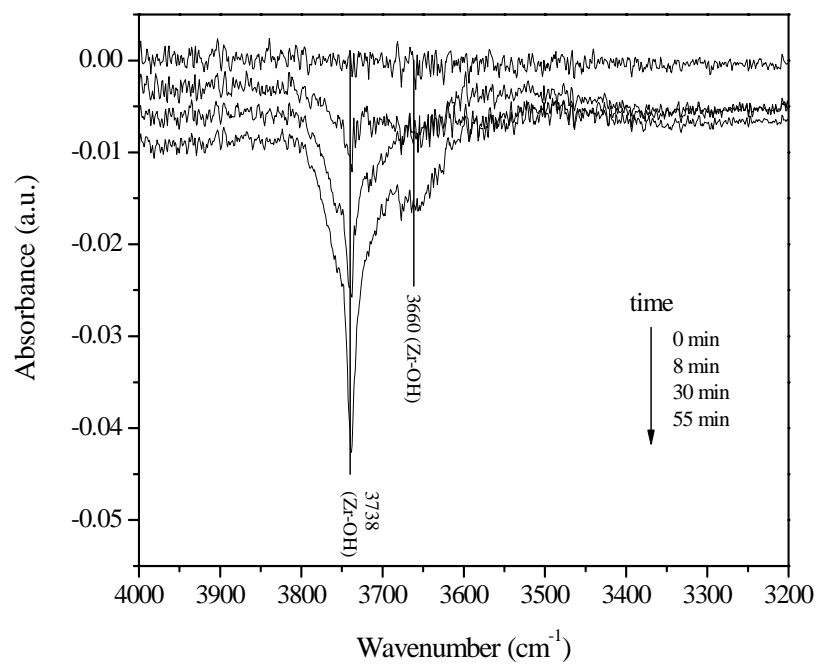


**Figure 2.** Infrared spectra (O-H stretching region) taken for 1.2 wt% Cu/t-ZrO<sub>2</sub> at 523 K after switching feed from 0.50 MPa He to 0.05 MPa CO and 0.45 MPa He flowing at a total rate of 60 cm<sup>3</sup>/min. Spectra referenced to 1.2 wt% Cu/t-ZrO<sub>2</sub> under 0.50 MPa He flow at 523 K.

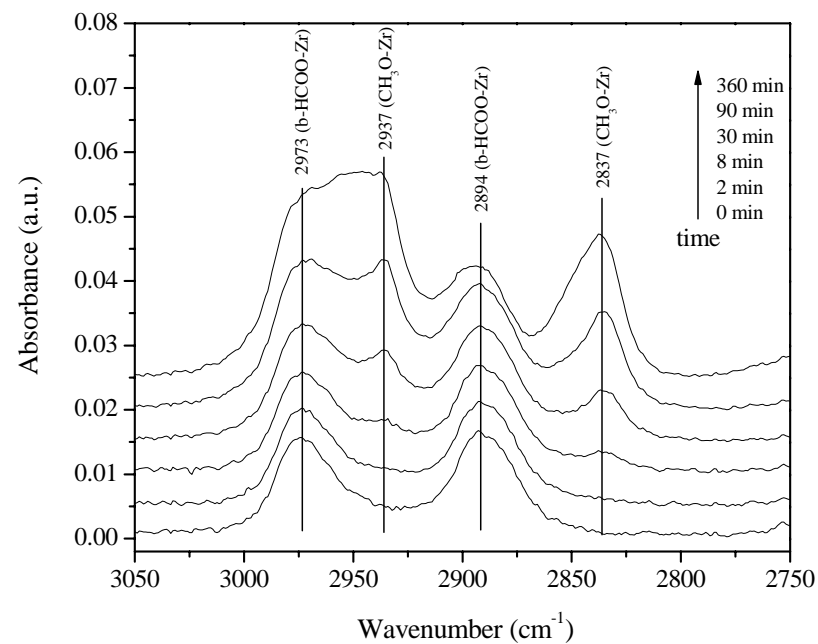
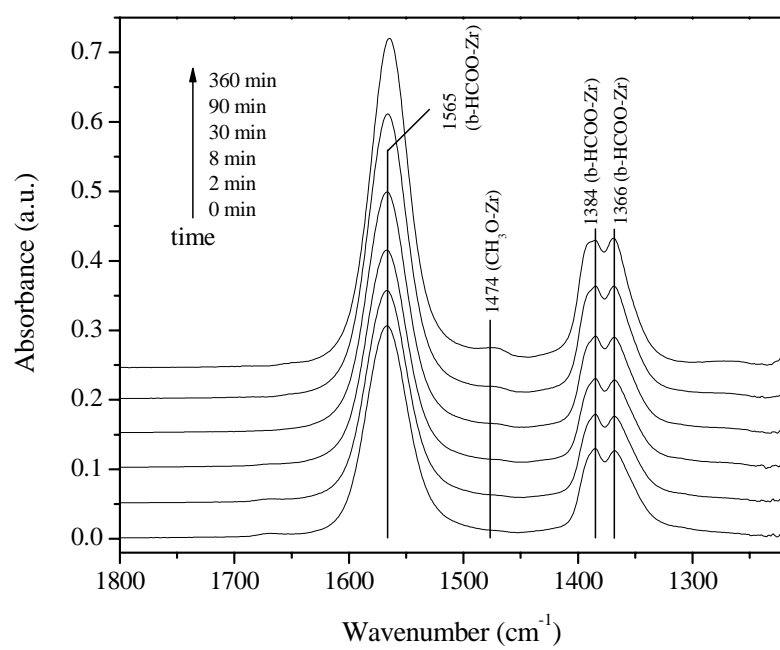


**Figure 3.** Infrared spectra taken for 1.2 wt% Cu/t-ZrO<sub>2</sub> at 523 K after switching feed from 0.05 MPa CO and 0.45 MPa He to 0.05 MPa CO, 0.15 MPa H<sub>2</sub>, and 0.30 MPa He flowing at a total rate of 60 cm<sup>3</sup>/min. Spectra referenced to 1.2 wt% Cu/t-ZrO<sub>2</sub> under 0.50 MPa He flow at 523 K.

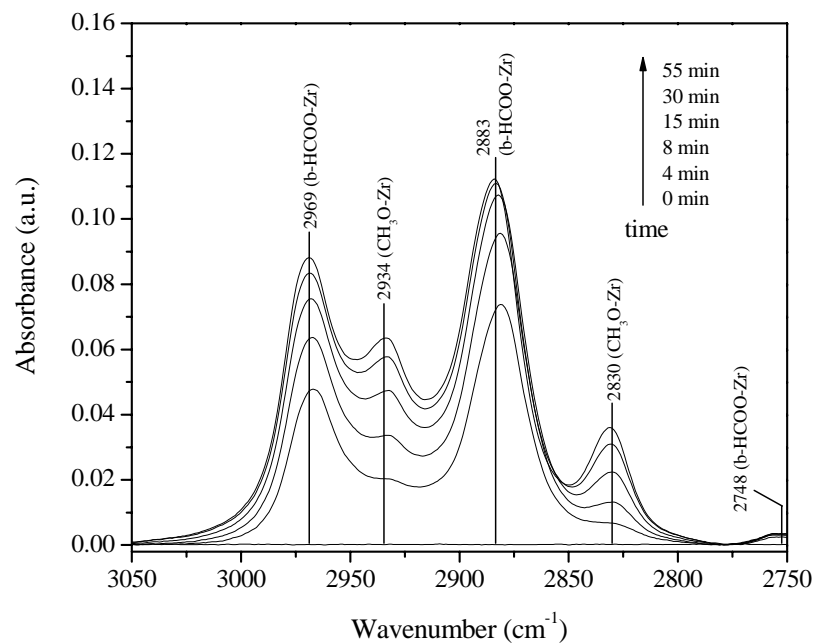
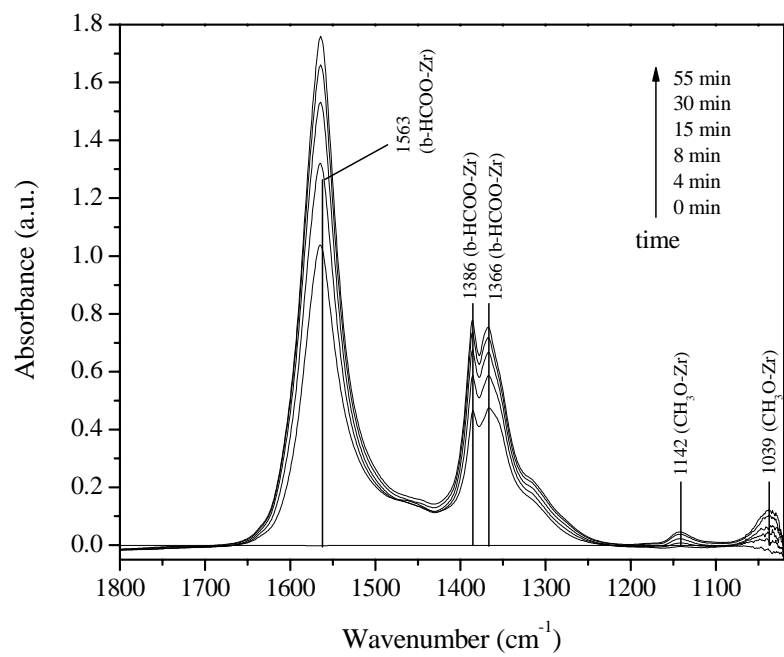


**Figure 4.** Infrared spectra taken for 1.2 wt% Cu/m-ZrO<sub>2</sub> at 523 K after switching feed from 0.50 MPa He to 0.05 MPa CO and 0.45 MPa He flowing at a total rate of 60 cm<sup>3</sup>/min. Spectra referenced to 1.2 wt% Cu/m-ZrO<sub>2</sub> under 0.50 MPa He flow at 523 K.

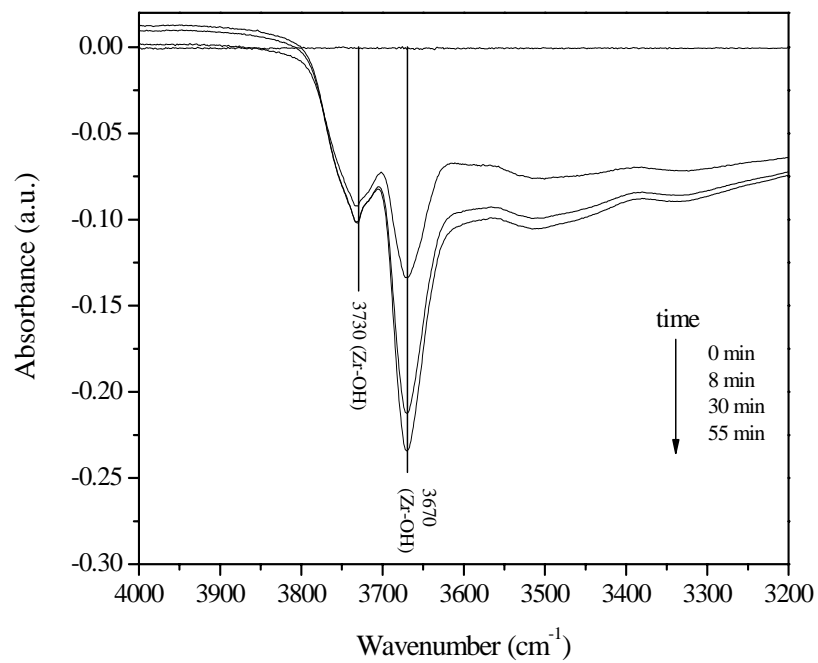


**Figure 5.** Infrared spectra taken for 1.2 wt% Cu/m-ZrO<sub>2</sub> at 523 K after switching feed from 0.50 MPa He to 0.05 MPa CO and 0.45 MPa He flowing at a total rate of 60 cm<sup>3</sup>/min. Spectra referenced to 1.2 wt% Cu/m-ZrO<sub>2</sub> under 0.50 MPa He flow at 523 K.

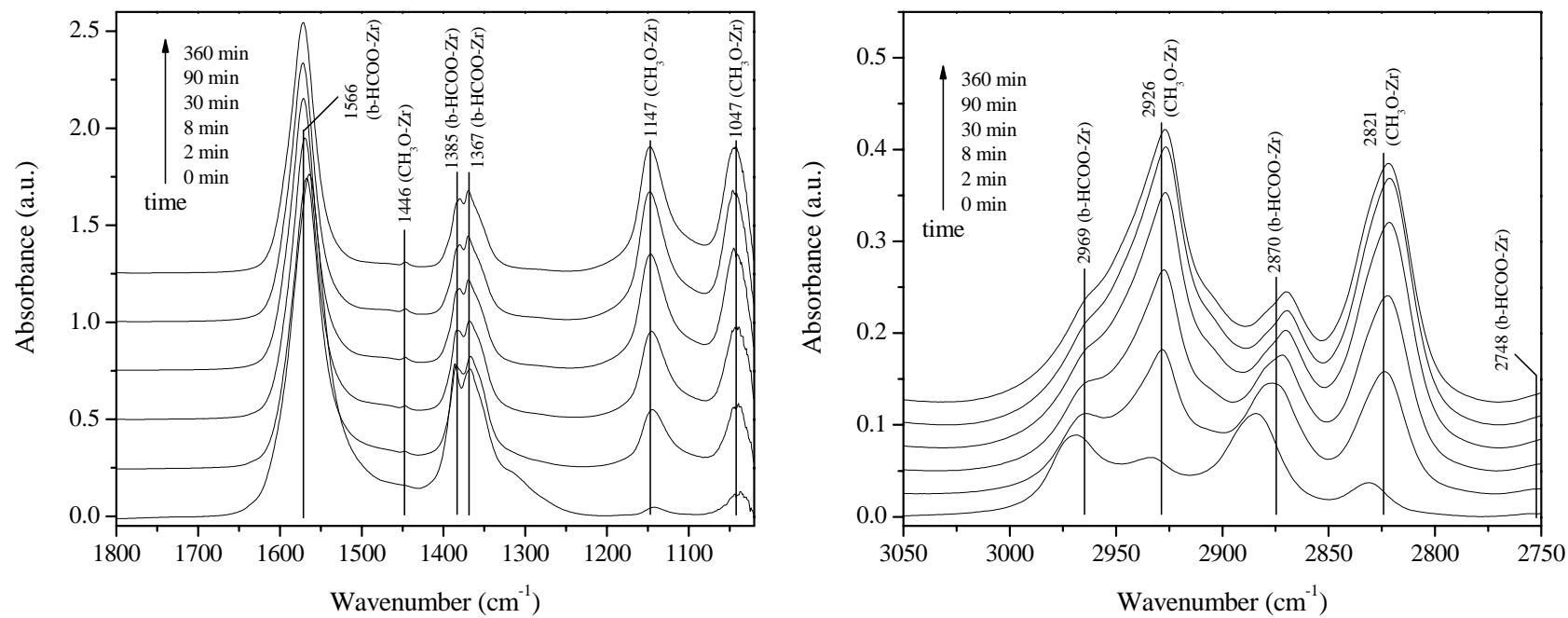


**Figure 6.** Infrared spectra taken for 1.2 wt% Cu/m-ZrO<sub>2</sub> at 523 K after switching feed from 0.05 MPa CO and 0.45 MPa He to 0.05 MPa CO, 0.15 MPa H<sub>2</sub>, and 0.30 MPa He flowing at a total rate of 60 cm<sup>3</sup>/min. Spectra referenced to 1.2 wt% Cu/m-ZrO<sub>2</sub> under 0.50 MPa He flow at 523 K.

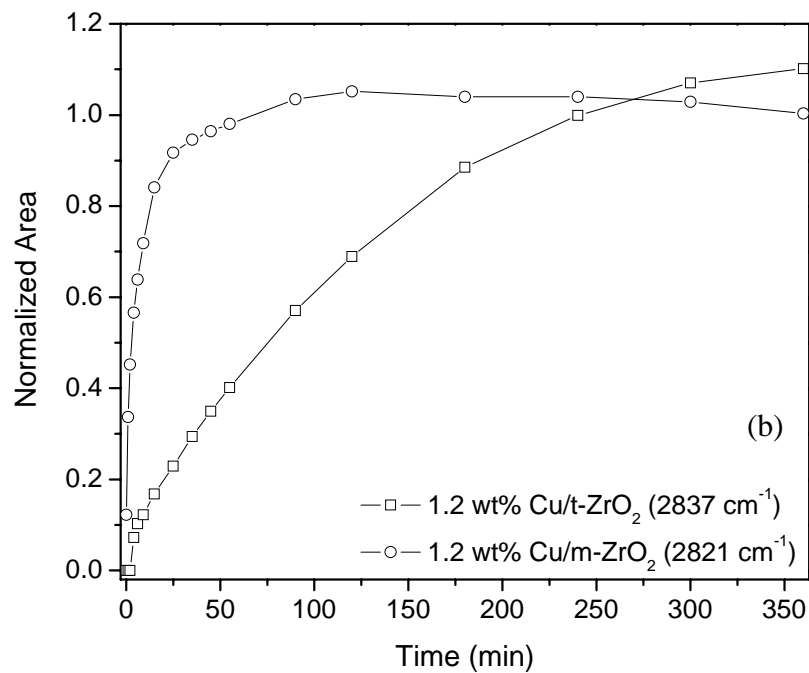
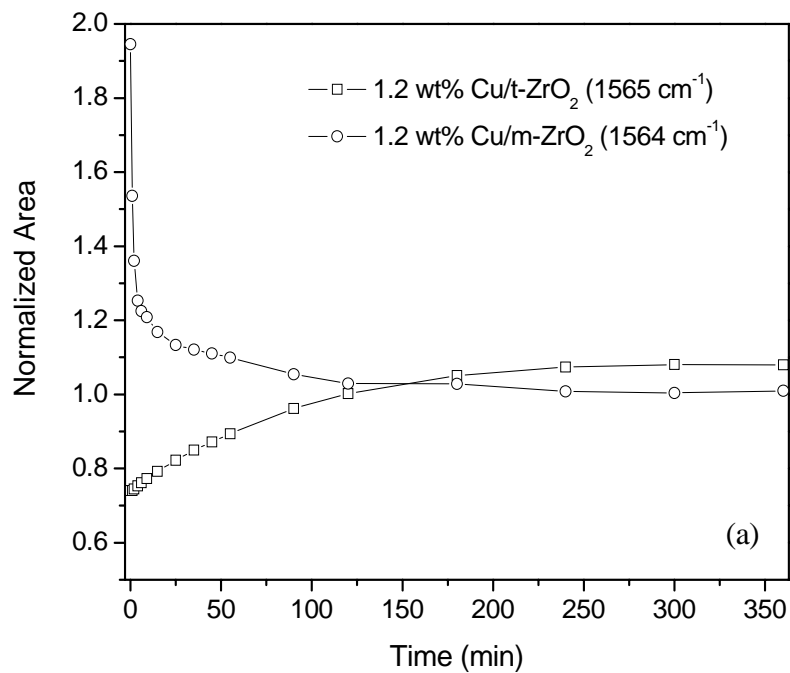


**Figure 7.** Relative IR peak intensities versus time for (a) b-HCOO-Zr and (b) CH<sub>3</sub>O-Zr observed for 1.2 wt% Cu/t-ZrO<sub>2</sub> and 1.2 wt% Cu/m-ZrO<sub>2</sub> during the experiments shown in Figs. 3 and 6. Areas normalized to the values observed at the end of the transient.

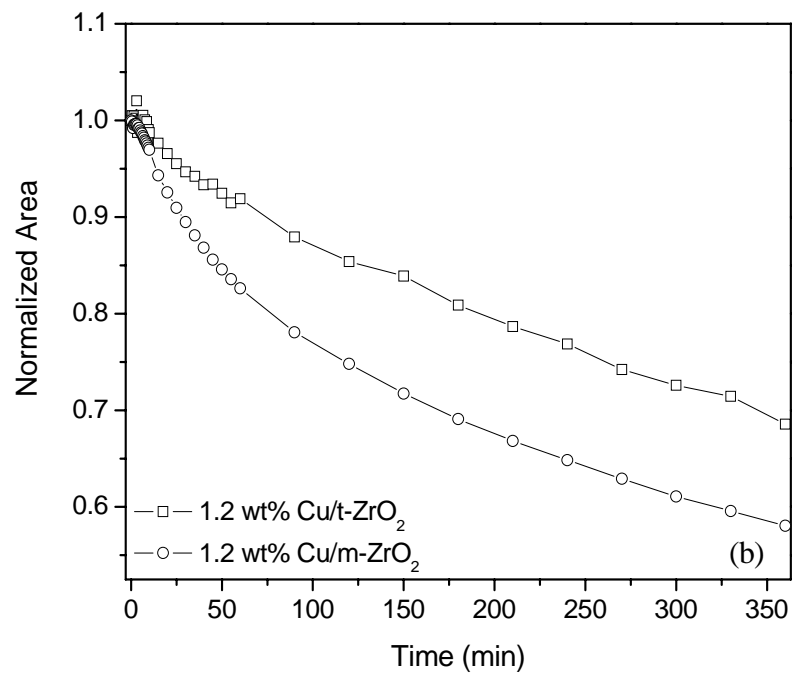
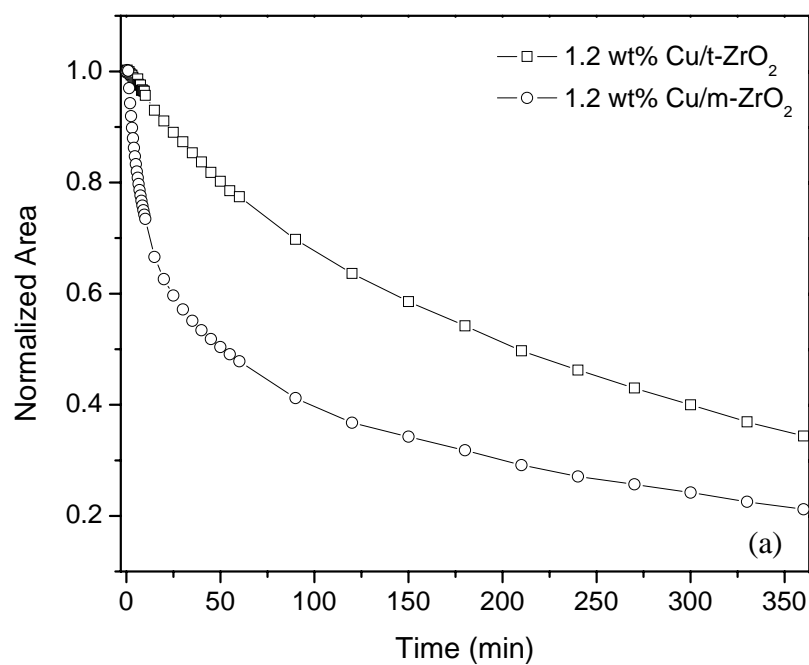


**Figure 8.** Relative IR peak intensities versus time for (a) b-HCOO-Zr, (b) CH<sub>3</sub>O-Zr, and (c) initial 20 min of (b) observed for 1.2 wt% Cu/t-ZrO<sub>2</sub>, and 1.2 wt% Cu/m-ZrO<sub>2</sub> at 523 K after switching feed from 0.05 MPa CO, 0.15 MPa H<sub>2</sub>, and 0.30 MPa He to 0.15 MPa H<sub>2</sub> and 0.35 MPa He flowing at a total rate of 60 cm<sup>3</sup>/min. Areas normalized to the values observed at the beginning of the transient.

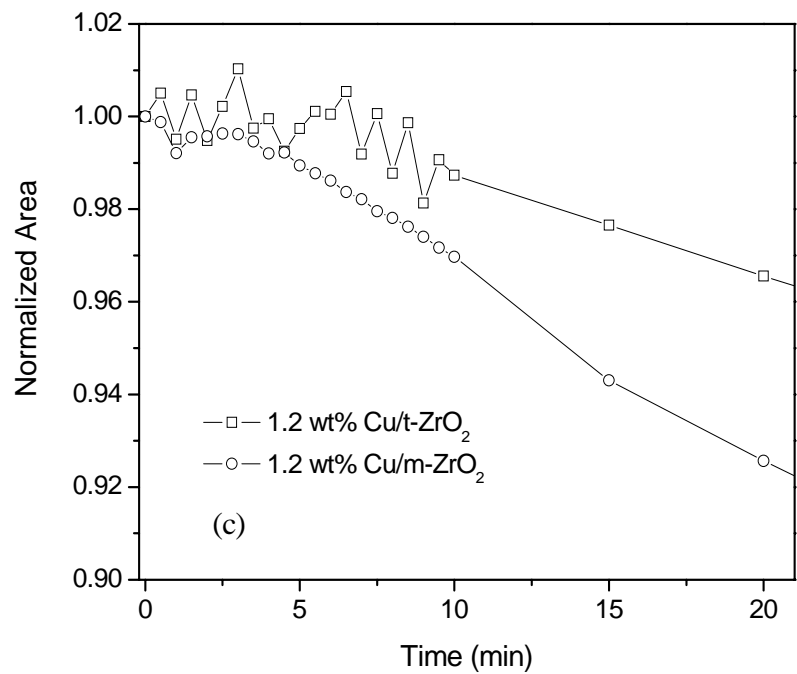


**Figure 8.** Relative IR peak intensities versus time for (a) b-HCOO-Zr, (b) CH<sub>3</sub>O-Zr, and (c) initial 20 min of (b) observed for 1.2 wt% Cu/t-ZrO<sub>2</sub>, and 1.2 wt% Cu/m-ZrO<sub>2</sub> at 523 K after switching feed from 0.05 MPa CO, 0.15 MPa H<sub>2</sub>, and 0.30 MPa He to 0.15 MPa H<sub>2</sub> and 0.35 MPa He flowing at a total rate of 60 cm<sup>3</sup>/min. Areas normalized to the values observed at the beginning of the transient.

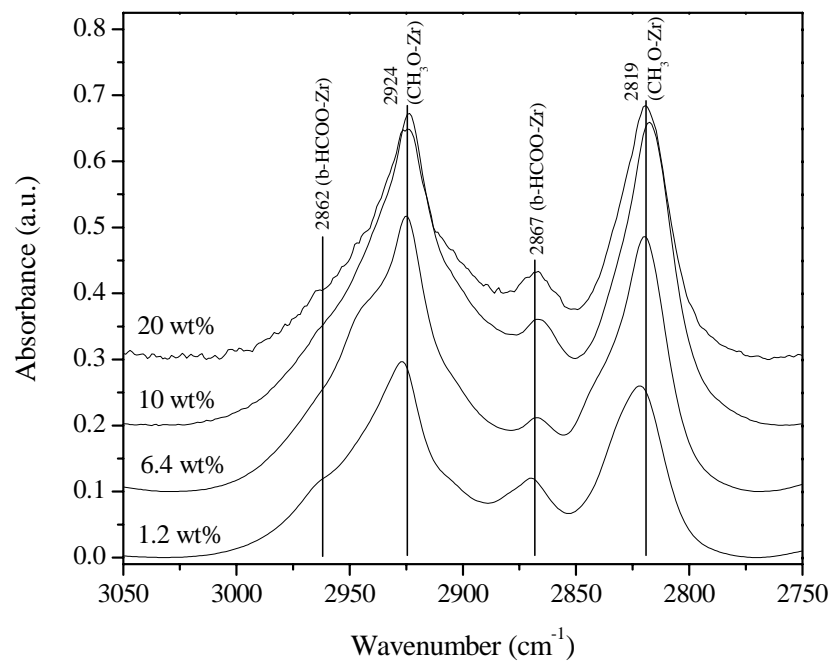
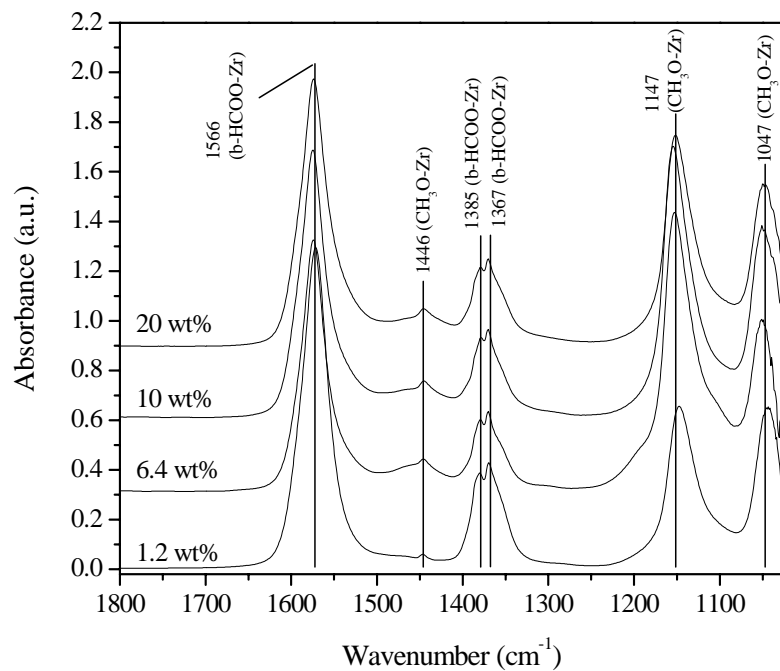


**Figure 9.** Infrared spectra taken for 1.2, 6.4, 10, and 20 wt% Cu/m-ZrO<sub>2</sub> at 523 K after switching feed from 0.05 MPa CO to 0.45 MPa He to 0.05 MPa CO, 0.15 MPa H<sub>2</sub>, and 0.30 MPa He flowing at a total rate of 60 cm<sup>3</sup>/min. Spectra referenced to 1.2, 6.4, 10, and 20 wt% Cu/m-ZrO<sub>2</sub> under 0.50 MPa He flow at 523 K, respectively.

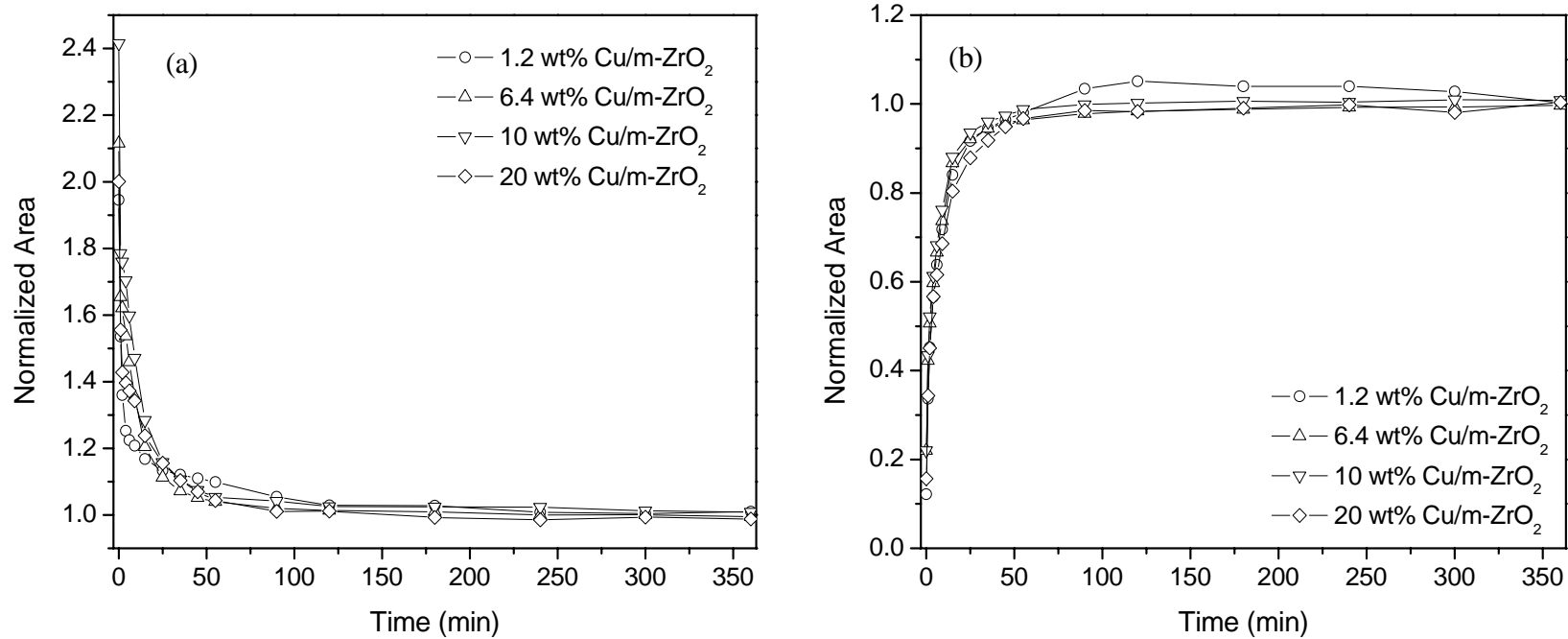


**Figure 10.** Relative IR peak intensities of (a) b-HCOO-Zr and (b) CH<sub>3</sub>O-Zr features for 0, 1.2, 6.4, 10, and 20 wt% Cu/m-ZrO<sub>2</sub> during the experiments in Fig. 9. Areas normalized to the values observed at the end of the transient.

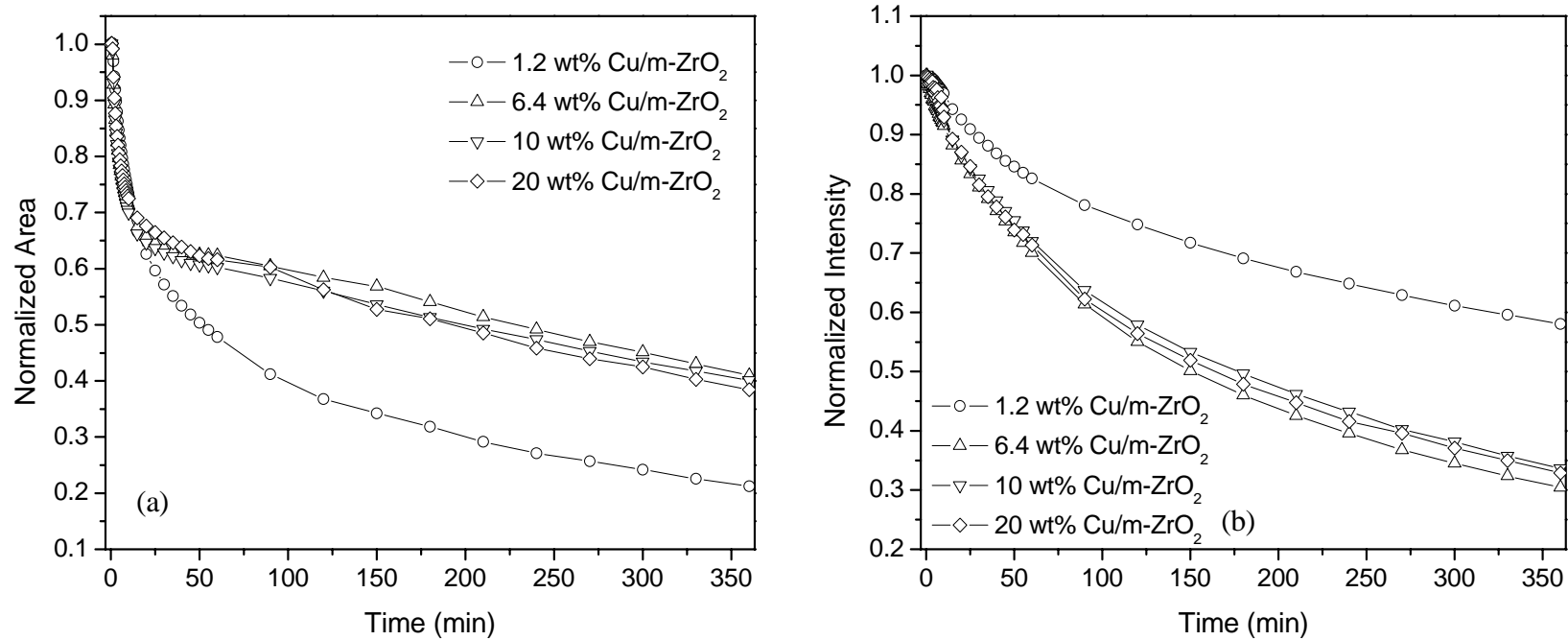


**Figure 11.** Relative IR peak intensities of (a) b-HCOO-Zr, (b) CH<sub>3</sub>O-Zr, and (c) initial 20 min of (b) features for 0, 1.2, 6.4, 10, and 20 wt% Cu/m-ZrO<sub>2</sub> at 523 K after switching feed from 0.05 MPa CO, 0.15 MPa H<sub>2</sub>, and 0.30 MPa He to 0.15 MPa H<sub>2</sub> and 0.35 MPa He flowing at a total rate of 60 cm<sup>3</sup>/min. Areas normalized to the values observed at the beginning of the transient.

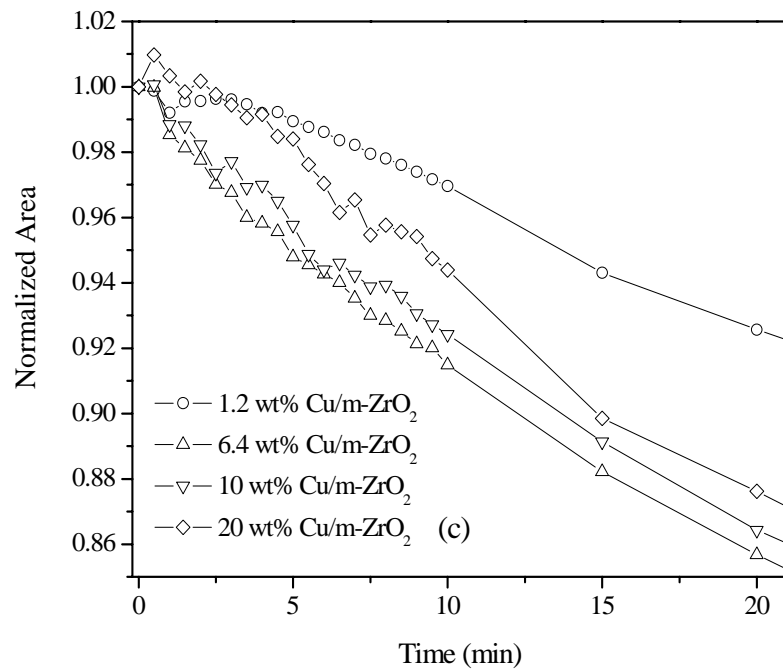


**Figure 11.** Relative IR peak intensities of (a) b-HCOO-Zr, (b) CH<sub>3</sub>O-Zr, and (c) initial 20 min of (b) features for 0, 1.2, 6.4, 10, and 20 wt% Cu/m-ZrO<sub>2</sub> at 523 K after switching feed from 0.05 MPa CO, 0.15 MPa H<sub>2</sub>, and 0.30 MPa He to 0.15 MPa H<sub>2</sub> and 0.35 MPa He flowing at a total rate of 60 cm<sup>3</sup>/min. Areas normalized to the values observed at the beginning of the transient.

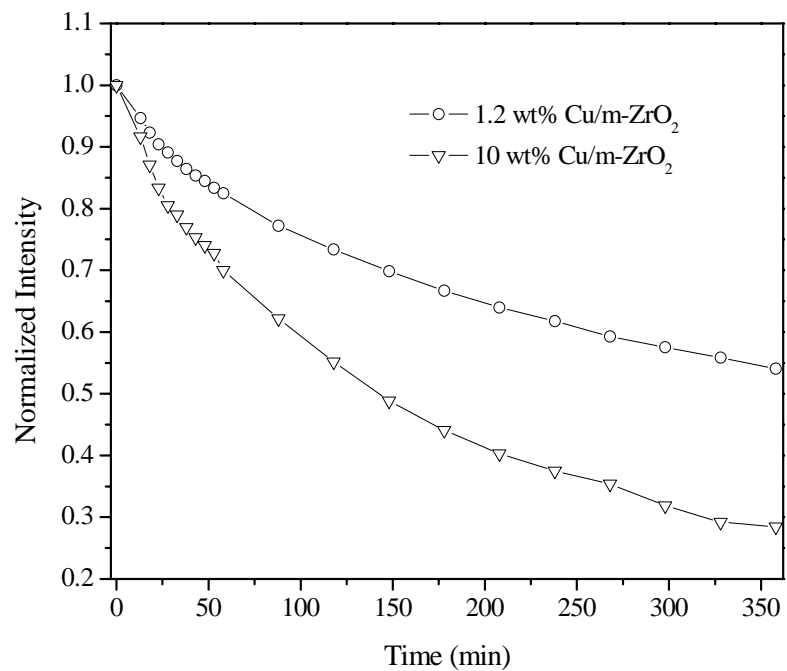


**Figure 12.** Relative IR peak intensities of CH<sub>3</sub>O-Zr features for 1.2 and 10 wt% Cu/m-ZrO<sub>2</sub> at 523 K after switching feed from 0.0025 MPa CH<sub>3</sub>OH and 0.4975 MPa He to 0.15 MPa H<sub>2</sub> and 0.35 MPa He flowing at a total rate of 60 cm<sup>3</sup>/min. Areas normalized to the values observed at the beginning of the transient.

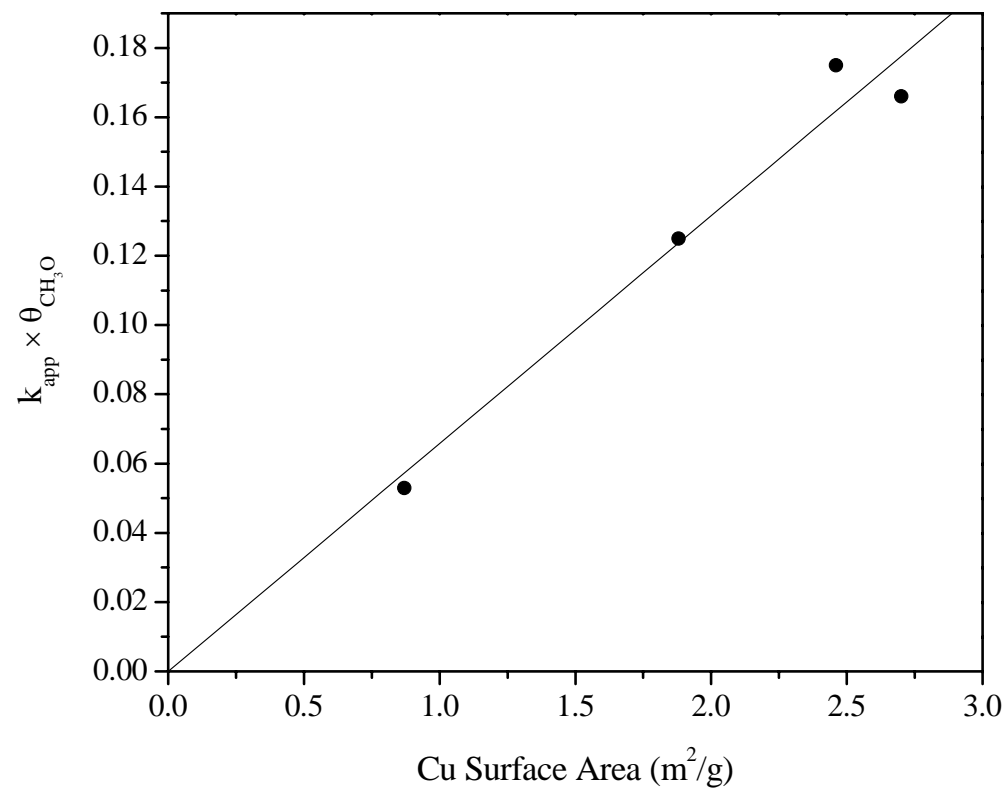


**Figure 13.** Product of apparent first-order rate coefficient for CH<sub>3</sub>O-Zr removal and CH<sub>3</sub>O-Zr peak area versus Cu surface area for each Cu/m-ZrO<sub>2</sub> sample.